

The Origin of Fermi Arcs in Underdoped High-Temperature Superconductors

Mike Guidry⁽¹⁾, Yang Sun⁽²⁾, and Cheng-Li Wu⁽³⁾

⁽¹⁾*Department of Physics and Astronomy, University of Tennessee, Knoxville, Tennessee 37996–1200*

⁽²⁾*Department of Physics, University of Notre Dame, Notre Dame, IN 46556*

⁽³⁾*Physics Department, Chung Yuan Christian University, Chung-Li, Taiwan 320, ROC*

(Dated: February 10, 2019)

Angle-resolved photoemission spectroscopy indicates that a full Fermi surface exists in the pseudogap region of cuprate superconductors if the temperature T lies above the pseudogap temperature T^* . However, below T^* only arcs of the Fermi surface survive, scaling as T/T^* as $T \rightarrow 0$. We show here that the SU(4) model leads microscopically to the origin and doping dependence of the T^* scale, and to a quantitative, parameter-free description of Fermi arcs. Our results strongly constrain theories of the pseudogap, and suggest that loss of nodal and antinodal Fermi surfaces may proceed by similar mechanisms.

Angle-resolved photoemission spectroscopy (ARPES) [1, 2] probes electronic properties [1, 3] of pseudogap (PG) states in high-temperature superconductors [4, 5]. Leading-edge ARPES gaps suggest decreased state density near the Fermi energy for temperature T less than the PG temperature T^* , and are anisotropic in momentum with strong T -dependence. A full Fermi surface exists for $T > T^*$; as the temperature decreases below T^* , only arcs centered on the nodal lines survive [6, 7, 8], scaling as T/T^* to zero length for $T \rightarrow 0$ [8].

Earlier theoretical work on Fermi arcs has employed a variety of approaches, including precursor pairs [9, 10], the perturbative renormalization group [11], high-temperature expansions in the t - J model [12], RVB models with strong gauge coupling [13], and time-reversal violating phases [14], but there is no agreed-upon explanation of Fermi arcs. The issue has received renewed focus because of recent comprehensive results by Kanigel, et al [8] that place the strongest constraints yet on the nature of Fermi arcs.

In earlier work we have proposed an SU(4) model to calculate the ground state properties of cuprate systems. Generalized SU(4) coherent states are the simplest Hartree–Fock–Bogoliubov variational solutions that incorporate antiferromagnetism (AF) competing with d -wave superconductivity on a lattice with no double occupancy [15, 16, 17, 18, 19, 20]. They generalize BCS to incorporate AF self-consistently. If AF correlations vanish, the SU(4) gap equations reduce to the BCS gap equations; if instead singlet pairing vanishes, the SU(4) gap equations describe an AF spin system with Néel order at half filling; for finite AF and SC correlations, the SU(4) gap equations describe the evolution with doping (P) and temperature (T) of d -wave Cooper pairs interacting with strong AF correlations.

SU(4) states forbid double occupancy by symmetry, not by projection [18]. The exact zero- T ground state at half filling is an AF Mott insulator that evolves rapidly with hole doping into a superconductor with strong AF correlations in the underdoped region, and finally into a singlet, d -wave superconductor beyond a critical hole doping $P_q \simeq 0.16$ – 0.19 [19]. At finite T for $P > P_q$, pairing is reduced by thermal fluctuations and the pairing gap vanishes at T_c . In the underdoped region ($P < P_q$) there are quantum fluctuations associated with AF correlations in addition to thermal fluctuations at

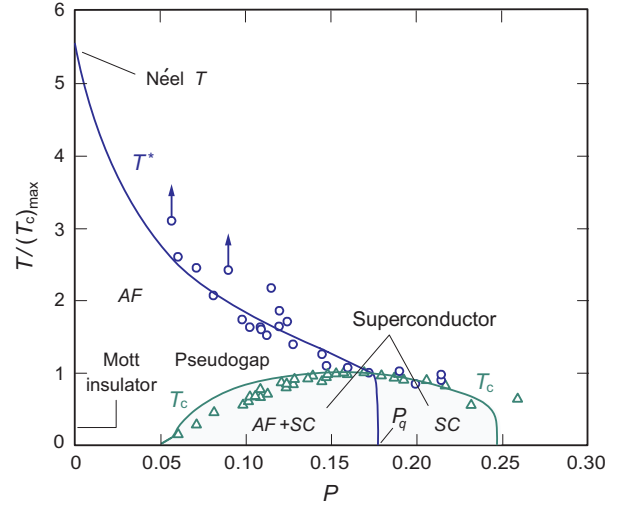


FIG. 1: SU(4) cuprate phase diagram compared with data. Strengths of the AF and singlet pairing correlations were determined by global fits to cuprate data [19, 20]. The PG temperature is T^* and the SC transition temperature is T_c . The AF correlations vanish, leaving a pure singlet d -wave condensate, above the critical doping P_q . Dominant correlations in each region are indicated by italic labels. Data from Refs. [22, 23, 24, 25, 26, 27, 28] (arrows indicate lower limits).

finite T . The interplay between AF, pairing, and thermal fluctuations produces PG states above T_c in which the fermionic pairs interact through AF correlations. Thus the SU(4) model identifies the energy gap Δ_q opened by the AF correlations as the pseudogap, while the (singlet and triplet fermion) pairs in these states may be viewed as d -wave preformed pairs. The SU(4) model can reproduce both the pseudogap and pairing gap with doping dependence quantitatively in agreement with data (see Ref. [20]). The SC transition temperatures T_c and PG transition temperatures T^* are also well reproduced, as illustrated in Fig. 1. This is our first significant finding: SU(4) coherent states give microscopic descriptions of pairing gaps and pseudogaps, and their transition temperatures T_c and T^* , that are in quantitative agreement with cuprate data.

The 16 generators $\{\mathcal{G}_i\}$ of $U(4) \supset SU(4)$ are [15, 16, 17,

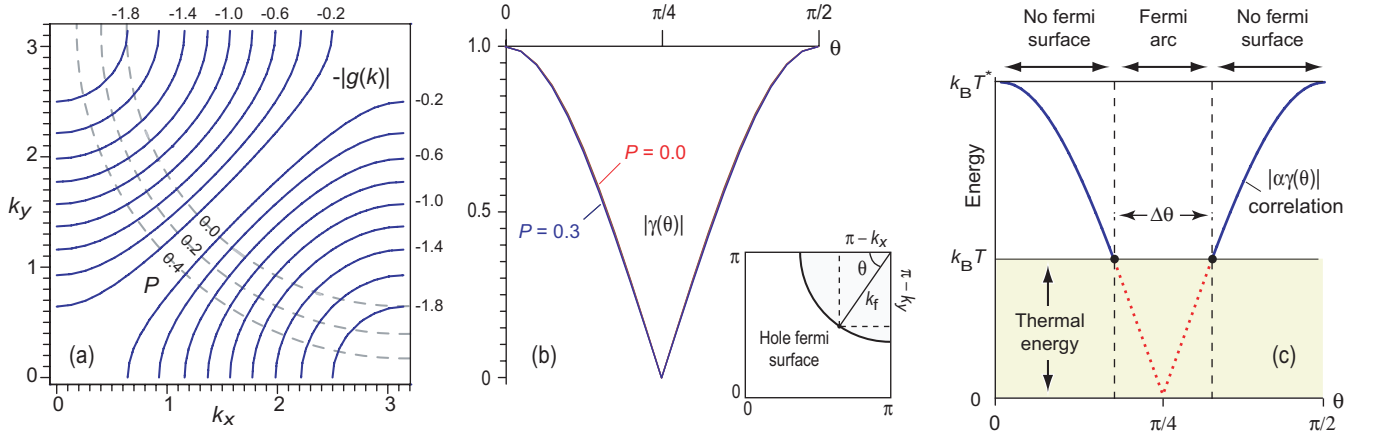


FIG. 2: The \mathbf{k} anisotropic factor, pseudogap correlation energy, and graphical Fermi-arc solution. (a) The k anisotropic factor $|g(k)|$ (blue lines) and contours of equal hole doping P (dashed gray lines), in the first Brillouin zone. (b) Correlation energy $\alpha\gamma(\theta)$ for unit $\alpha = kT^*$ evaluated along the Fermi surface [curves of constant P in part (a)] as a function of the angle θ (defined in inset). Curves corresponding to doping $P = 0 - 0.3$ lie almost on top of each other, indicating that $\gamma(\theta)$ is largely insensitive to doping. (c) Graphical solution of the Fermi-arc problem. The curve defines the PG correlation energy and horizontal lines correspond to constant thermal energy scales $k_B T$ associated with a given temperature T . Their intersections (black dots) represent points in the momentum space where the pseudogap is just closed by thermal fluctuations; these bracket arcs $\Delta\theta$ of surviving Fermi surface.

18, 19, 20]

$$\begin{aligned} D^\dagger &= \sum_k g(k) c_{k\uparrow}^\dagger c_{-k\downarrow}^\dagger, & \pi_{ij}^\dagger &= \sum_k g(k) c_{k+q,i}^\dagger c_{-k,j}^\dagger \\ Q_{ij} &= \sum_k c_{k+q,i}^\dagger c_{k,j}, & S_{ij} &= \sum_k c_{k,i}^\dagger c_{k,j} - \frac{1}{2} \Omega \delta_{ij} \end{aligned} \quad (1)$$

and hermitian conjugates, where $\uparrow\downarrow$ or (i, j) are spin indices taking two values, $q \equiv \mathbf{q} = (\pi, \pi, \pi)$, and the d -wave pair formfactor is

$$g(k) = g(k_x, k_y) = \cos k_x - \cos k_y, \quad (2)$$

with $k \equiv \mathbf{k} = (k_x, k_y)$. These operators are summed over momentum k . They are appropriate for describing data that are not momentum-selected (for example, Fig. 1). However, ARPES Fermi-arc data exhibit explicit dependence on k . The SU(4) formalism may be extended to deal with this case by viewing the individual k components of the operators defined in Eq. (1) as the symmetry generators:

$$\{\mathcal{G}(k)\} \equiv \{D^\dagger(k), D(k), \bar{\pi}^\dagger(k), \bar{\pi}(k), \bar{Q}(k), \bar{S}(k), n_k\} \quad (3)$$

where, for example, the singlet pair generator D^\dagger in Eq. (1) is related to the k -dependent singlet pair generators $D^\dagger(k)$ in Eq. (3) by

$$D^\dagger = \sum_{k>0} D^\dagger(k).$$

Instead of the global SU(4) symmetry generated by Eq. (1), the symmetry now is a direct product of k -dependent SU(4) groups, $\prod_{k>0} \otimes \text{SU}(4)_k$. The corresponding Hamiltonian is

$$\begin{aligned} H &= \sum_{k>0} \epsilon_k n_k - \sum_{kk'} \{ \chi_{kk'} \bar{Q}(k) \cdot \bar{Q}(k') \\ &\quad + G_{kk'}^{(0)} D^\dagger(k) D(k') + G_{kk'}^{(1)} \bar{\pi}^\dagger(k) \cdot \bar{\pi}(k') \}, \end{aligned} \quad (4)$$

with interaction strengths

$$\chi_{kk'} = \chi^0 |g(k)g(k')| \quad G_{kk'}^{(i)} = G^{(i)} \delta_k \delta_{k'} \quad (i = 0, 1), \quad (5)$$

where $\delta_k = |g_0(k)|$, the maximum value of $g(k)$, except that $\delta_k = 0$ at the nodal point.

We shall term this k -dependent formalism the $\text{SU}(4)_k$ model. All results of the original k -independent SU(4) model of Refs. [15, 16, 17, 18, 19, 20] (including those of Fig. 1) are recovered as a special case of the $\text{SU}(4)_k$ model when $k = k_f$ in the anti-nodal direction ($\theta = 0, \pi/2$ in Fig. 2), which gives the maximum energy gaps and their transition temperatures. However, general solutions of the $\text{SU}(4)_k$ model give new k -anisotropic properties. Of direct relevance to the present discussion is that the temperature for the PG closure $T^*(k)$ becomes anisotropic in k ; specifically, we derive in the $\text{SU}(4)_k$ model

$$T^*(k) = T^* \left| \frac{g(k_f)}{g_0} \right| \quad (6)$$

where g_0 is the maximum value of $g(k_f)$ and T^* is the PG temperature of the k -independent SU(4) model plotted in Fig. 1 (corresponding to the maximum value of $T^*(k)$); the explicit form of T^* may be found in Eq. (49) of Ref. [19]. See Ref. [21] for details. Equation (6) defines the full temperature and doping dependence of Fermi arcs. The ultimate physical reason for this result is that the singlet and triplet pairs interacting by AF interactions in the SU(4) PG state each carry a $g(k)$ formfactor, which introduces a k dependence in the effective AF coupling and thus in T^* .

In Fig. 2(a) we show the behavior of $g(k)$ as a function of (k_x, k_y) . The components (k_x, k_y) in $g(k_f)$ are constrained by the Fermi surface. Assuming an isotropic hole surface [dashed

gray lines in Fig. 2(a)], we have

$$(\pi - k_x)^2 + (\pi - k_y)^2 = k_f^2 = 2\pi(1 + P) \quad (7)$$

(we consider a more realistic Fermi surface below). For a given doping P (thus k_f) and temperature T , with $T^*(k) = T$ by virtue of Eq. (6) under the constraint (7), we obtain the angles θ_1 and θ_2 at which the PG closes (the angle θ is defined in the inset to Fig. 2), and the length of the surviving Fermi arc is $k_f|\theta_2 - \theta_1| \equiv k_f\Delta\theta$.

This result may be interpreted graphically. In Fig. 2(b) we show $\gamma(\theta) \equiv |g(k_f)/g_0|$ versus angle θ along different Fermi surfaces [dashed gray lines in Fig. 2(a)]. We see that $\gamma(\theta)$ is almost independent of doping P . Thus, solving Eq. (6) with the Fermi surface constraint (7) is equivalent to solving

$$k_B T^*(k) = \alpha \gamma(\theta) \quad \alpha = k_B T^*. \quad (8)$$

The correlation energy $\alpha\gamma(\theta)$ associated with the PG depends on the k direction θ [Fig. 2(c)]. The pseudogap closes when the thermal excitation energy $k_B T$ is comparable to the PG correlation energy. The intersections of horizontal lines of fixed $k_B T$ with the correlation energy curve [black dots in Fig. 2(c)] define Fermi-arc solutions θ_1 and θ_2 . Outside those points (solid blue curve), the correlation energy is larger than the energy of thermal fluctuations (shaded in green), the PG opens, and the Fermi surface is gapped. Inside these points (dotted red curve), the thermal energy exceeds the correlation energy, the PG closes, and the Fermi surface exists in an arc $\Delta\theta$ between the dots. When $T > T^*$, the PG is closed in all directions and there is a full Fermi surface since $k_B T > \alpha$ and α is the maximum PG correlation energy.

The arc solution exemplified graphically in Figs. 2(b)–(c), or algebraically in Eq. (6), is our second significant finding: For given temperature T , the anisotropy of $\gamma(\theta)$ partitions the k -space uniquely into regions having a Fermi surface [$T > T^*(\theta)$] and those that do not [$T < T^*(\theta)$]. As Fig. 2(c) suggests, arc lengths decrease with decreasing T at fixed doping, with a full Fermi surface at $T = T^*$ but only the nodal points at $T = 0$. Doping dependence enters primarily through the maximum PG temperature T^* and the Fermi momentum k_f ; the temperature dependence enters through T/T^* . For fixed T , arcs shrink toward the nodal points with decreased doping because T^* in T/T^* increases at smaller doping (Fig. 1). However, if Fermi-arc length is measured by the fraction $\Delta\theta/(\pi/2)$ and the temperature is scaled by T^* , the weak doping dependence of $\gamma(\theta)$ ensures that $\Delta\theta/(\pi/2)$ versus T/T^* is almost independent of doping and compound.

Kanigel, et al [8] report fractional arc lengths versus T/T^* for Bi2212 that we plot in Fig. 3. Our theoretical solution for the fractional arc lengths [obtained from Fig. 2(c) or Eq. (6)] is the solid line in Fig. 3; agreement between data and theory is remarkable, given that the theoretical curve has no adjustable parameters and that we can *predict* the scale T^* implicit in the data with the same theory (Fig. 1). Note that the qualitatively different behavior at high and low temperatures in Fig. 3 (rapid drop in arc length for decreasing $T \sim T^*$, shifting to

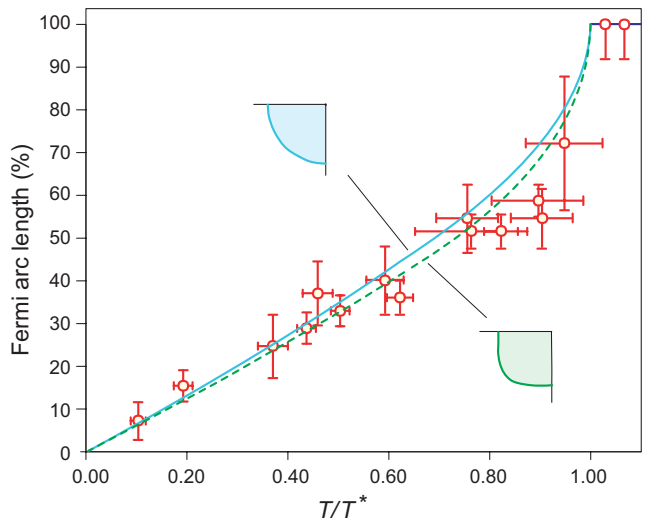


FIG. 3: Fermi arc length versus temperature. Experimental arc length is displayed as a percentage of the full Fermi surface length versus T/T^* for underdoped Bi2212 [8]; the solid curve is our prediction for an isotropic Fermi surface (inset upper left); the dashed curve assumes a Fermi surface with flat antinodal segments (inset lower right). No parameters were adjusted in either calculation and the curves are almost independent of doping.

approximately linear decrease to zero arc-length at $T = 0$), is explained entirely by geometry in Fig. 2(c).

Realistic cuprate Fermi surfaces have flat segments near zone boundaries. This will not alter the present discussion substantially. The dashed curve in Fig. 3 uses the Fermi surface shown inset lower right. The small difference between dashed and solid curves indicates that arc solutions depend only weakly on differing curvature in the nodal and antinodal parts of the Fermi surface. Absolute arc lengths depend on doping and temperature. However, the scaled arc lengths of Fig. 3 are *near-universal functions only of the ratio T/T^** , largely independent of compound, doping, and Fermi surface details, as data suggest.

Figure 3 illustrates our third significant finding: agreement between theory and data with no parameter adjustment suggests that our SU(4) formalism outlines a complete solution of the Fermi-arc mystery. We now argue that this has important implications for understanding pseudogap behavior.

The data in Fig. 3 have been interpreted [8] as representing a rapid drop from a full Fermi surface at $T = T^*$, destroying the antinodal Fermi surface at essentially constant temperature, followed by a linear decrease of Fermi-arc length with decreasing T/T^* on the near-nodal region of the Fermi surface, extrapolating to zero arc length at the nodal points for $T/T^* \rightarrow 0$. This suggests that nodal and antinodal Fermi surfaces may be removed differently as T is lowered (see Ref. [29]). For example, it has been argued [8] that abrupt removal of the antinodal surface at $T \simeq T^*$ may be associated with a lattice vector connecting antinodal surfaces (Ref. [29] speculates that gapping of the antinodal surface may be associ-

ated with charge ordering), while the linearly-varying removal of the nodal regions extrapolating to a nodal-point surface at $T = 0$ may support a nodal liquid picture [30].

The present results invite simpler hypotheses. Our unified, parameter-free analysis suggests that Fig. 3 is consistent with removal of both nodal and antinodal surfaces by the *same mechanism*. Therefore, the qualitatively different variation of arc length with T/T^* in nodal and antinodal regions is not sufficient to indicate that loss of Fermi surface proceeds by different mechanisms in these regions. Nor do the data of Ref. [8] imply unique support for nodal liquids. We have demonstrated specifically that the SU(4) model accounts quantitatively for Fermi arcs and T^* , without invoking nodal liquids.

Our results show that a theory of Fermi arcs must make two correct predictions: (1) $T^*(k) \propto \gamma(\theta)$, and (2) the scale T^* and its doping dependence. *Any theory* having a $T^*(k)$ consistent with Eq. (8) can account for the scaled data of Fig. 3, if T^* is taken from data. Hence, our fourth significant finding: scaled ARPES data (Fig. 3) test whether a pseudogap has a nodal structure similar to that of the superconducting state, which favors theories that relate the structure of superconducting and pseudogap states. But discriminating among different theories meeting this condition requires more: a quantitative description of how the Fermi surface is lost and of the PG temperature scale T^* and its doping dependence (Fig. 1), all obtained self-consistently. We conclude that only a highly-restricted set of models can be consistent with the aggregate properties of Fermi arcs. The SU(4) model was shown here to meet this stringent criterion; it is of interest whether other models can do likewise.

We thank Elbio Dagotto, Pengcheng Dai, and Takeshi Egami for extensive discussion and helpful comments, and Elbio Dagotto for calling our attention to an error in our original formulation.

-
- [1] M. R. Norman and C. Pépin, Rep. Prog. Phys. **66**, 1547 (2003).
 - [2] A. Damascelli, A. Hussain, and Z.-X. Shen, Rev. Mod. Phys. **75**, 473 (2003).
 - [3] E. Dagotto, Rev. Mod. Phys. **66**, 763 (1994).
 - [4] T. Timusk, and B. Statt, Rep. Prog. Phys. **62**, 61 (1999).
 - [5] M. Norman, D. Pines, and C. Kollin, Adv. Phys. **54**, 715 (2005).
 - [6] M. R. Norman, et al, Nature **392**, 157 (1998).
 - [7] X.-J. Zhou, et al, Phys. Rev. Lett. **92**, 187001 (2004).
 - [8] A. Kanigel, et al, Nature Phys. **2**, 447 (2006).
 - [9] J. R. Engelbrecht, A. Nazarenko, M. Randeria, and E. Dagotto, Phys. Rev. **B57**, 13406 (1998).
 - [10] G. Preosti, Y. M. Vilck, and M. R. Norman, Phys. Rev. **B59**, 1474 (1999).
 - [11] N. Furukawa, T. M. Rice, and M. Salmhofer, Phys. Rev. Lett. **81**, 3195 (1998).
 - [12] W. O. Putikka, M. U. Luchini, and R. R. P. Singh, Phys. Rev. Lett. **81**, 2966 (1998).
 - [13] X. G. Wen, and P. A. Lee, Phys. Rev. Lett. **80**, 2193 (1998).
 - [14] C. M. Varma, and L. Zhu, arXiv:cond-mat/0607777.
 - [15] M. W. Guidry, Rev. Mex. Fís. **45 S2**, 132 (1999).
 - [16] M. W. Guidry, L.-A. Wu, Y. Sun, and C.-L. Wu, Phys. Rev. **B63**, 134516 (2001).
 - [17] L.-A. Wu, M. W. Guidry, Y. Sun, and C. L. Wu, Phys. Rev. **B67**, 014515 (2003).
 - [18] M. W. Guidry, Y. Sun, and C.-L. Wu, Phys. Rev. **B70**, 184501 (2004).
 - [19] Y. Sun, M. W. Guidry, and C.-L. Wu, Phys. Rev. **B73**, 134519 (2006).
 - [20] Y. Sun, M. W. Guidry, and C.-L. Wu, Phys. Rev. **B75**, 134511 (2007).
 - [21] Y. Sun, M. W. Guidry, and C.-L. Wu, submitted to Phys. Rev. **B**; arXiv:0705.0818v1 [cond-mat.supr-con]
 - [22] P. Dai, et al, Science **284**, 1344 (1999).
 - [23] M. Oda, et al, Physica **C281**, 135 (1997).
 - [24] T. Watanabe, et al, Phys. Rev. Lett. **84**, 5848 (2000).
 - [25] J. C. Campuzano, et al, Phys. Rev. Lett. **83**, 3709 (1999).
 - [26] J. Wuyts, V. V. Moshchalkov, and Y. Bruynseraede, Phys. Rev. **B53**, 9418 (1996).
 - [27] M. Takigawa, et al, Phys. Rev. **B43**, 247 (1991).
 - [28] T. Ito, K. Takenaka, and S. Uchida, Phys. Rev. Lett. **70**, 3995 (1993).
 - [29] K. McElroy, Nature Phys. **2**, 441 (2006).
 - [30] L. Balents, M. P. A. Fisher, and C. Nayak, Int. J. Mod. Phys. **B12**, 1033 (1998).